Granular Matter (2021) 23:17
https://doi.org/10.1007/s10035-020-01060-8

ORIGINAL PAPER

Stress based multi-contact model for discrete-element simulations

K. Giannis[1,2] · C. Schilde[1,2] · J. H. Finke[1,2] · A. Kwade[1,2] · M. A. Celigueta[3] · K. Taghizadeh[4,5] · S. Luding[4]

Received: 16 August 2019 / Accepted: 19 September 2020 / Published online: 19 February 2021

Abstract
The aim of this study is to introduce a stress-based non-binary contact model missing in classical discrete element method (DEM). To tackle this issue, a classical force-displacement contact law is generalized by utilizing the trace of the particle stress tensor to make all contacts dependent on all other contacts of a particle and thus, to account for multiple contacts simultaneously acting on a single particle. Simulation results for uniaxial confined (oedometric) compression employing our new multi-contact model were compared with the classical discrete element formulation, an existing strain-based multi-contact model, and experimental data. The satisfactory agreement between these results supports the validity of our new contact model. Several test examples at higher load levels show that our generalized contact model is able to capture the stronger non-linearity at higher stresses. Due to its simplicity, the proposed multi-contact model can easily be integrated in any DEM implementation, remaining relatively fast when compared to more complex methods or even a discretization of particles, e.g. by FEM.

Keywords Discrete element method · Multi-contact method · Stress tensor · Deformable particles · Large deformation

1 Introduction

Granular media, such as sand, are ensembles of dissipative, athermal grains that interact through repulsive and frictional contact forces. An interesting feature of granular materials is the fact that they can behave as solids or liquids, and show peculiar mechanical properties like dilatancy, history dependence, ratcheting and anisotropy [1, 2]. Despite their simplicity and omnipresence, the physics of granular materials is still not fully understood and this leaves many open questions in different fields, e.g. physics, process engineering, material science, geotechnical engineering, etc.

The discrete element method (DEM), pioneered by Cundall and Strack [3], models granular materials numerically as a collection of particles rather than as a continuum, and the bulk behaviour of granular materials depends on the collective interactions among individual particles. Each discrete element has its own individual movement that can be traced by explicitly integrating the governing differential equation based on Newton's second law of motion.

DEM has been used in a wide variety of applications such as powders [4], ceramics [5], granular flows [6], pharmaceutical and food industries [7, 8]. Despite the fact that DEM is a very efficient tool to study these applications, modeling of confined, high to extreme compression with DEM is still a challenge. In classical DEM, the so-called soft particle approach [9], particle deformations are mimicked by overlaps between contacting particles. When an overlap is detected, the contact forces between two particles are calculated by a contact law. The general assumption made is that contacts between particles are independent and therefore, contact forces are resolved locally. This assumption is only true in cases when particles deformation is small. For cases with large deformations classical DEM is limited on capturing the required deformation [10, 11].

✉ K. Giannis
k.giannis@tu-braunschweig.de

1 Institute for Particle Technology (iPAT), Technische Universität Braunschweig (TUBS), Volkmaroder Str. 5, 38104 Braunschweig, Germany

2 Center of Pharmaceutical Engineering (PVZ), Technische Universität Braunschweig (TUBS), Franz-Liszt-Str. 35A, 38106 Braunschweig, Germany

3 Centre Internacional de Metodes Numerics a l'Enginyeria (CIMNE), Barcelona, Spain

4 Multi-Scale Mechanics, TFE, ET, MESA+, University of Twente, 7500 AE Enschede, The Netherlands

5 Institute of Applied Mechanics (CE), SC SimTech, University of Stuttgart, Stuttgart, Germany

One way to introduce deformability in a particle model is by applying the Multiple Particle Finite Element Method (MPFEM) [12, 13] where each individual particle is being meshed with finite elements. Another way is to combine FEM and DEM [14, 15], a method that embodies contact detection algorithms of DEM in the framework of FEM. Particle deformability can be also modeled with other continuum based dicretization methods such as the material point method (MPM) [16–19] or the bonded particle method (BPM) [20]. The main advantage of these methods is their ability to deal with anisotropic deformations of single particles. Therefore, these models are able to model arbitrary shapes after deformation. However, the main challenge is their high computational cost that hinders their use for cases with a large number of particles.

Following a different strategy, there have been attempts to introduce deformable particles in the framework of DEM. A simple approach proposed by Haustein et al. [21] that expands the radius of the spherical particles. The particle deformation from its overlapping area is redistributed on the free surface of the particle, such that the volume of the particle is kept constant. A sophisticated model was proposed by Rojek et al. [22], the so-called deformable discrete element method (DDEM). In this approach, particles are uniformly deformed under uniform internal stress, which generates a uniform strain inside the particle; and contact forces are evaluated using the local and newly formed global overlap caused by the deformation of the particle.

The need of having deformable particles in the framework of DEM has led to the formulation of the multi-contact discrete element method (MC-DEM). Brodu et al. [23] incorporated explicitly the mutual influence of contacts acting simultaneously on a single particle. In this method, the overall deformation of a particle is evaluated in terms of the strain field induced by other contacts acting on the particle. Brodu et al. compared the results of conventional DEM, their new model, and experimental results for uniaxial compression of hydrogel particle packings in order to show the ability of their model to reproduce the real physical data. Furthermore, the evolution of the microstructure, using the multi-contact approach, was compared against the nonlocal contact formulation presented by Gonzalez et al. [24].

Another idea is to employ the stress instead of the strain field in calculations. For this reason, a multi-body contact law that accounts for contact dependency was presented by Frenning [25]. In this case, particle deformation is approximated by truncated spheres; and the contact force was expressed as the product of the sum of normal stresses (independent of contacts direction) and a contact area (that differs between the pair of contacts). The contact dependency among contacts acting on the same particle was also considered in the work of Celigueta et al. [26]. However, in this case the contact dependency was restricted to contacts acting perpendicular to the contact direction considered. Lastly, the contact dependency on individual grains are also considered in the granular element method (GEM) presented by Karanjgaokar [27]. The GEM method, in order to obtain inter-particle forces, involves a multi-objective optimization problem that includes momentum balance, stress-force relations, and constraint equations.

This study proposes a new formulation in the context of multi-contact discrete element methods based on the stresses acting on single particles to account for multiple contact effects. In the following, our model is called MC-stress since our formulation utilizes the trace of the stress tensor acting on a single particle. The multi-contact model proposed from Brodu et al. will be called MC-strain, since in this case the main feature is the strain field around particles. At this point, it is necessary to highlight the similarities and differences with respect to the MC-strain proposed by Brodu et al. The main difference between the new methodology and the MC-strain is that the new model is based on the stress applied on the particle not the strain. The MC-strain model estimates the particle deformations by using analytical formulas given by elasticity theory, based on similar assumptions, but conjugate variables as the MC-stress model. In both models, the overall deformation of a particle is calculated and this deformation is then used for the calculation of the new contact forces. The MC-strain model takes into account a pseudo geometric deformation resulting form the strain field that is surrounding the particle. Fundamentally, this method is iterative at each simulation step. The ideal case would be to iterate the forces applied at each contact until convergence. However, in order to accelerate the computations, the hypothesis is made that grains move slowly and quasi-static at the scale of an elementary time step, so that a single iteration shall be sufficient. Nevertheless, we have noticed that an iteration procedure is inevitable for cases of fast compression and with large applied engineering strain. Since, for these cases, the particles acceleration which is introduced by the MC-strain model at a next time step is enormous and can cause instabilities. On the contrary, with MC-stress the deformation is corrected by utilizing the momentary stress state experienced by the particle to calculate the newly generated contact forces. Based on the outcome of this study we can say that MC-stress model is more "economical" compared with MC-strain when it comes to the extra forces experienced by a particle and subsequently a more stable calculation is expected. Lastly, significant difference between the two models is their complexity resulting in variance in the computational cost. As it is shown in this research, the MC-stress model performs faster compared with the single iteration MC-strain model. We expect that for fast compression a single iteration within MC-strain is not sufficient, hence, the computational time will rise further. This outcome is crucial for large scale industrial application (e.g. tableting) where the gain in computational cost can save up to days of simulations.

This paper is organized as follows: in the second section, the classical discrete element method is presented. A general overview on the existing multi-contact model proposed by Brodu et al. is given in section three. Furthermore, the formulation and implementation of our new multi-contact model is presented followed by a case with a single compressed rubber sphere and at the end of section three, test cases with collisions of three and five particles are considered to show how the multi-contact models are performing in comparison to classical DEM. In section four, cases of uni-axial compaction using hydrogel balls are presented. Additionally, a numerical test on a harder material (rubber spheres) is given and a case of uniaxial compaction using stiff material, glass beads, is successfully tested. Finally, the computational cost of the performance of the multi-contact models is discussed. We conclude our work in the last section; and finish with some outlooks.

2 Discrete element method

The approach towards the microscopic understanding of macroscopic particulate material behaviour is the modelling of particles using the so-called discrete element method (DEM), a numerical scheme originally formulated and developed by Cundall et al.

DEM is a straightforward implementation to solve the transitional and rotational equations of motion for a system of many interacting particles:

$$m_i\ddot{\mathbf{a}}_i = \mathbf{f}_i + m_i\mathbf{g} \qquad I_i\dot{\boldsymbol{\omega}}_i = \boldsymbol{\tau}_i \tag{1}$$

where m_i is the mass, $\ddot{\mathbf{a}}_i$ is the acceleration and $\mathbf{f}_i$ is the total particle's force of the ith particle with position $\mathbf{x}_i$. It is subjected to two kinds of forces, one due to contacts with other particles ($\mathbf{f}_i = \sum_c \mathbf{f}_i^c$) and one due to volume forces (i.e. gravity acceleration, $\mathbf{g}$ which is neglected in this study, I_i is the spherical particles moment of inertia, $\dot{\boldsymbol{\omega}}_i$ is the angular velocity and $\boldsymbol{\tau}_i = \sum_c(\mathbf{l}_i^c \times \mathbf{f}_i^c + \mathbf{q}_i^r + \mathbf{q}_i^t)$ is the total torque, where $\mathbf{l}_i^c$ is the branch vector and $\mathbf{q}_i^r$, $\mathbf{q}_i^t$ are torques due to rolling and torsion.

The basis of DEM are force laws that relate the interaction force to the overlap of two particles. The contact force can be decomposed into a normal and tangential component $\vec{f}_i^c = \vec{f}^n + \vec{f}^t$. With the normal and tangential forces acting on all particles, one can numerically integrate the equations of motion and obtain the next position of particles. Below, we describe a force law used in this research.

2.1 Normal contact law

The elementary units of granular material are mesoscopic grains which deform under contact forces, induced by an externally applied stress. For realistic modelling of the deformation of particles we relate the interaction force to the overlap δ of two particles. Note that the evaluation of the inter-particle forces based on the overlap may not be sufficient to account for the inhomogeneous stress distribution inside the particles. Two particles i and j, with radii r_i and r_j and positions $\mathbf{x}_i$ and $\mathbf{x}_j$ only interact if they are in contact, resulting in an overlap:

$$\delta^n = (r_i + r_j) - (\mathbf{x}_i - \mathbf{x}_j)\cdot\mathbf{n} > 0, \tag{2}$$

where $\mathbf{n} = \frac{\mathbf{x}_i - \mathbf{x}_j}{|\mathbf{x}_i - \mathbf{x}_j|}$ is the unit vector pointing from particle j to particle i.

In Eq. (1), the contact force is needed to determine the particle trajectory. This force is calculated through a contact force law, which is a simplification of the contact between two particles. The Hertzian contact model is the most common used contact model in DEM which is a non-linear model based on the Hertz theory of elastic contacts [28–30]. This model assumes that the particles are spherical and do not deform during the simulation. In addition, this model considers binary contacts between two particles which means particles are in contact through a single point during their collisions. The normal contact force model involves normal repulsive (f_{el}^n) and normal dissipative force (f_{visc}^n):

$$f^n = f_{el}^n + f_{visc}^n = \frac{4}{3}E^*\sqrt{r_{ij}\delta^n}\delta^n + \eta^n\sqrt{r_{ij}\delta^n}\dot{\delta}^n \tag{3}$$

with $r_{ij} = \frac{r_i r_j}{r_i + r_j}$ as the effective radius and E^* is the effective Young's modulus, $\frac{1}{E^*} = \frac{1-\nu_i}{2G_i} + \frac{1-\nu_j}{2G_j}$. In this expression, ν and G represent the particles Poisson's ratio and shear modulus, respectively. In reality, particles collisions are inelastic, i.e. energy loss occurs during collisions. Here, the dissipation is related to relative velocity in normal direction ($v_{rel}^n = -(\mathbf{v}_i - \mathbf{v}_j)\cdot\mathbf{n} = \dot{\delta}^n$) of interacting particles with the viscoelastic damping constant for normal contact viscosity η^n which is an intrinsic material parameter. Dissipation should be improved based on [31] but this is beyond the scope of this study.

2.2 Tangential force law

Modeling the tangential forces that arise from oblique particle impacts has elicited a considerably wider range of force models than those of normal interactions [32–34]. Here, the tangential force is modeled like in the theory of Mindlin [35]. When two contacting surfaces are subject to an increasing tangential displacement, δ^t, then relative slip is initiated at the perimeter and progresses inward over an annular area of the contact surface. The incremental tangential force Δf^t due to the incremental tangential displacement $\Delta\delta^t$ depends not only on the loading history but also on the variation of

the normal force. Therefore, the incremental tangential force is obtained from the following equation:

$$f^{t+\Delta t} = f^t + \Delta f^t \tag{4}$$

where $f^{t+\Delta t}$ is the new and f^t is the old tangential force.

An approach based on the constant normal force solution of Mindlin was proposed by Tsuji et al. [36]. This approach is based on a linear tangential spring, k^t, with a stiffness coupled non-linearly to the normal displacement and was applied to a study on plug flow. Although strictly speaking, the proposed tangential model is only valid in case of a fully elastic material, it was combined with the non-linear viscoelastic model without adjusting any parameter [37]. Hence, the incremental tangential force is calculated as:

$$\Delta f^t = \Delta f^t_{el} + \Delta f^t_{visc} = k^t \Delta\delta^t + \eta^t \Delta v^t \tag{5}$$

with $k^t = 8G^*\sqrt{r_{ij}\delta^n}$. G^* is the effective shear modulus, $\frac{1}{G^*} = \frac{2-\nu_i}{G_i} + \frac{2-\nu_j}{G_j}$, δ^n is the relative normal displacement. Like in the normal direction, we consider a dissipation term along the tangential direction, using a viscosity η^t [38] which is combined with the change of velocity along the tangential direction Δv^t.

The elastic tangential displacement, $\Delta\delta^t$, between spheres, obtained by integrating surface relative tangential velocities during elastic deformation of the contact and given as [39, 40]:

$$\Delta\delta^t = \int_t^{t+\Delta t} v^t dt \longrightarrow \Delta\delta^t \cong v^t \Delta t \tag{6}$$

where v^t is the velocity component tangential to the contact surface and Δt is the time-step.

The tangential force is coupled to the normal force via Coulombs law, $f^t \leq \mu f^n$, where for the sliding case one has dynamic friction with $f^t = \mu f^n$. Here, the dynamic and the static friction coefficients are considered to be equal $\mu = \mu_d = \mu_s$. The static situation requires an elastic spring in order to allow for a restoring force, i.e., a non-zero remaining tangential force in static equilibrium due to activated Coulomb friction.

3 Deformable particle models

In the classical formulation of DEM, each contact force is considered to be a local phenomenon and it is resolved locally independent of the effect of other contact forces in its vicinity. However, in reality every contact between particles is affected by neighboring particles acting simultaneously. Deformation of particles induces non-linearity at the same and all other contacts, and can cause the formation of new contacts which is ignored in the conventional DEM approach. The essential ingredient is to consider an overall grain shape deformation induced by particle contacts.

Here, we adopt the nonlocal contact formulations that account for the interplay of deformations due to multiple contact forces acting on each single particle. Such nonlocal formulations remove the classical assumption that contacts acting on a single particle is formulated locally as independent of pair of particles interactions. In the following, we first explain a strain-based approach proposed by Brodu et al. and after that, we propose a new method, based on the stress and thus the elasticity of materials. Finally, we compare the explained models with the classical DEM results of simple test cases.

3.1 Multi-contact strain based model

To overcome the above summarized challenge, Brodu et al. proposed a multi-contact approach to improve the predictive power of DEM methods, while retaining their conceptual simplicity. In this approach, the mutual influence of contacts is modeled by using information on deformations induced by one contact force on the other contacts acting on the grain. The displacement fields imposed by neighboring contacts in normal direction, $\delta_{k\to c}$, are added to the particle deformation at the local contact, δ_c. After that, force calculation can be computed based on the added displacement fields $f_H \propto (\delta_c + \sum_k \delta_{k\to c})^{3/2}$ with the displacement fields $\delta_{k\to c}$ equal to:

$$\delta_{k\to c} = -\gamma \frac{(1+\nu) f_k^c}{2\pi E d_{kc}} \left[(\mathbf{n}_k \cdot \mathbf{u}_{kc})(\mathbf{n}_c \cdot \mathbf{u}_{kc}) \quad + \right.$$
$$\left. (3-4\nu)\mathbf{n}_k \cdot \mathbf{n}_c - (1-2\nu)\frac{(\mathbf{n}_k + \mathbf{u}_{kc}) \cdot \mathbf{n}_c}{1 + \mathbf{n}_k \cdot \mathbf{u}_{kc}} \right] \tag{7}$$

where f_k^c is the force at contact k, E is the Young's modulus of the material, and ν its Poisson's ratio. γ is an adjustable prefactor which accounts empirically for the geometry.

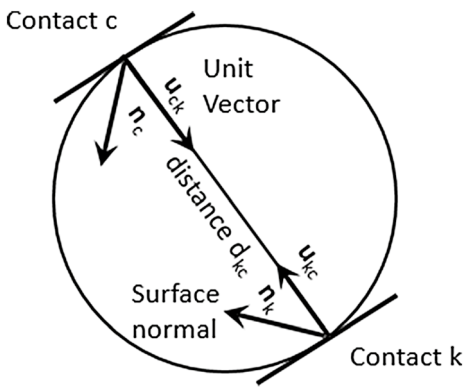

Fig. 1 Influence of one contact onto another. Contacts are not restricted to the surface of a sphere, their position is consistent with the grain deformations [23]

For incompressible materials (Poisson's ratio $\nu \to 0.5$) the prefactor is set to be $\gamma = 0.5$ and for compressible materials (Poisson's ratio $\nu \to 0$) $\gamma = 1$ [41]. d_{kc}, $\mathbf{n}$, and $\mathbf{u}_{kc}$ are the distance between contact points, normal vectors of contact surfaces, and unit vectors between contacts. These parameters are depicted in Fig. 1. Normal contact forces are calculated through this equation:

$$f_{el}^{n} = \frac{4}{3} E^{*} \sqrt{r_{ij}} (\delta^{n} + \sum_{k} \delta_{k \to c})^{\frac{3}{2}} \tag{8}$$

3.2 Multi-contact stress based model

In order to overcome the inherent assumption of the classical DEM which treats each contact locally as a binary pair-interaction, we propose a nonlocal model to describe a new space in which the mutual influence of contacts is taken into account. To do this, we took the advantage of the trace of the particle stress tensor and its information. The particle stress tensor $\boldsymbol{\sigma}^{p}$ by definition computes the stress level exerted on a particle by its neighboring particles after averaging the sum of all contact stresses within its volume [9, 42, 43]:

$$\boldsymbol{\sigma}^{p} = \frac{1}{V^{p}} \sum_{c=1}^{C^{p}} \mathbf{l}^{c} \otimes \mathbf{f}^{c} \tag{9}$$

where V_p is is the volume of the particle, C^P - number of contacts with neighboring particles, $\mathbf{l}^c$ - vector the so-called branch vector, $\mathbf{f}^c$ - force acting at the contact, and the dyadic product $\otimes$ of the two vectors leads to a tensor of rank two. The stress tensor incorporates multiple contacts on the particle. With that, we are able to collect information from all local contacts around a single particle to generalize the typical DEM normal force law in a way that the trace of the stress tensor is used for on-line calculations. In this concept, the new contact forces on each pair are depending also on the trace of the stress tensor of neighbouring particles, hence, an anisotropic deformation of a particle can be accounted for. Figure 2 depicts a schematic concept of the new approach. As it can be seen from the figure, an additional term is added into the conventional DEM (P_{ij}). This term consists of the trace of stresses applied on the primary (ith) particle ($\mathrm{tr}(\sigma_i)$), and the trace of stresses applied on the secondary (jth) particle ($\mathrm{tr}(\sigma_j)$).

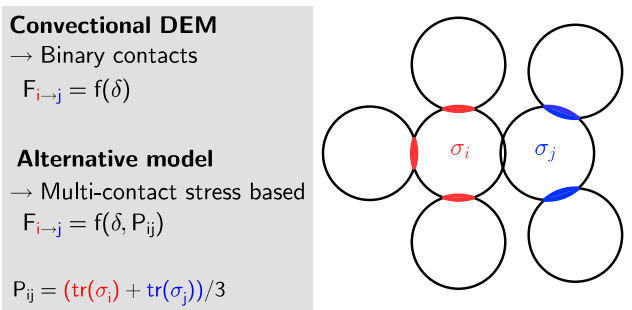

Fig. 2 For any pair-interaction, a term dependent on the average stress between particle i (red) and particle j (blue) is added to the normal force law (colour figure online)

A new term can be added into the former normal force calculation by including the trace of stress tensor:

$$f_{el}^{n} = \frac{4}{3} E^{*} \sqrt{r_{ij} \delta^{n}} \delta^{n} + (\beta \nu A_{ij}) P_{ij} \tag{10}$$

The first term in Eq. (10) was defined earlier (Eq. 3). The second term carries the information from neighboring particles acting on the particle. In this expression, β is an adjustable dimensionless empirical geometric prefactor that empirically accounts for the geometry of each particle, ν is the Poisson's ratio, and A_{ij} is the contact area at interface of the active pair of contacts. The isotropic component of the stress is the pressure $P_{ij} = \frac{1}{3}(\mathrm{tr}(\sigma_i) + \mathrm{tr}(\sigma_j))$, with $\mathrm{tr}(\sigma) = (\sigma_{xx} + \sigma_{yy} + \sigma_{zz})$.

The motivation for the relation between multi-contact correction term in Eq. 10 due to the present state of particles is manifold. (1) simplicity (i.e. simulation speed) by not taking into account every pair relative orientation, as in MC-strain model, and by avoiding iterations, (2) the material properties in the new formulations (Poisson's ratio $\nu = 0$ de-activates the model), (3) the contact geometry, A_{ij}, is computed before for each pair in contact, and (4) average stress which accounts the number and intensity of all the contacts around one particle.

The new multi-contact model, MC-stress, was implemented in the LIGGGHTS-DEM platform [44]. LIGGGHTS in its philosophy takes the benefit of Newton's third law, where forces are computed for each pair of particles once [45] in order to have an optimized and fast algorithm. By exploiting this, we can integrate our new formula without violating the momentum balance [$\mathbf{f}_{ij}^{c} = -\mathbf{f}_{ij}^{c}$]. In the "Appendix" the pseudo-code of the algorithm used is briefly described.

3.3 Uniaxial unconfined compression of a single rubber sphere

In order to validate the performance of the multi-contact formulations, we consider a uniaxial compression of an elastic rubber sphere of radius 1.0 cm and elastic properties which are given in Table 1 and compare the simulation results with experimental results from Tatara [46]. The sphere was pressed between two rigid plates as shown in Fig. 3 to a deformation up to $\frac{\delta}{r} = 0.4$ cm (40%). In Fig. 4 the results of the calibration are presented. As we can see Hertz theory is applicable only for small deformation with an upper limit of $\frac{\delta}{r} \leq 0.1$ (10%), whereas the multi-contact models, with $\gamma = 0.55$ and $\beta = 1.71$, show very good agreement with the

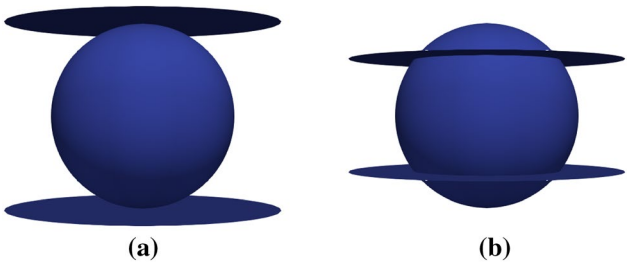

Fig. 3 Schematic representation of a rubber sphere uniaxially compressed between two rigid plates

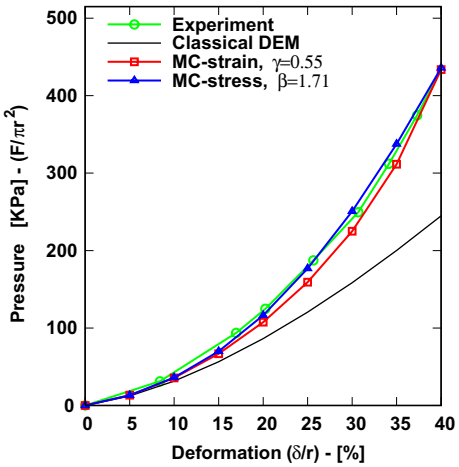

Fig. 4 Calibration of the multi-contact formulation with experimental data of a rubber spheres compressed between two rigid plates [46]

Table 1 Input parameters used for simulations from [21, 23, 24]

Material properties	Hydrogel	Rubber	Glass
Density ($\frac{kg}{m^3}$)	11.5	2000	2500
Diameter (cm)	2	2	0.4
Young's modulus (Pa)	23.3×10^3	1.85×10^6	65×10^9
Poisson's ratio (–)	0.5	0.46	0.24
Coefficient of restitution (–)	0.95	0.7	0.98
Friction coefficient (–)	0.03	0.5	0.2

experimental data for small up to large deformation. The maximum deformation point was used for calibration, so the data in-between validate the model behavior. Note that these parameters were calibrated in a way to not only capture the maximum force exerted on the top plate but also to follow the path during compression (and decompression when needed) of a rubber sphere.

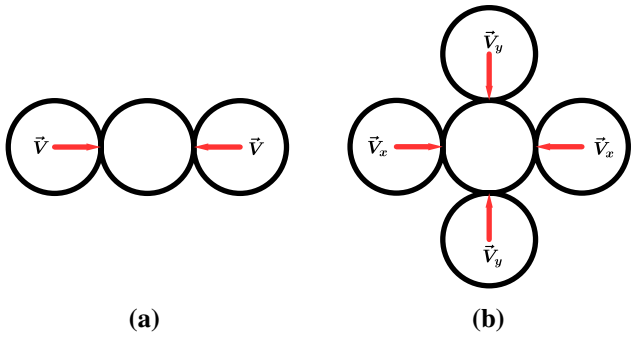

Fig. 5 Schematic representation of **a** three and **b** five particles interaction

3.4 Modeling test cases

To see the differences between given models and the classical DEM, we create a set of simple reference cases that includes a system of three and five particles. On the other hand, comparing results between the classical DEM, MC-strain, and MC-stress validates the implementation of MC-stress. Since the behavior of hydrogel grains was thoroughly examined in Refs. [23, 47], and it is the first material studied under the framework of multi-contact modeling, its material properties were used in this study. Moreover, we have used a harder (rubber) and a stiff (glass) material to further investigate the models. Material parameters used for the simulations are shown in Table 1.

It is clear that multi-contact models do not show any difference with the classical DEM in case of two sphere interactions. Therefore, the first reference case consists of a central sphere with a diameter of 2.0 cm that has been placed between two spheres with identical characteristics (see Fig. 5a). Initial velocities of 10 $\frac{m}{s}$ were applied in opposite directions such that the central sphere gets compressed, i.e. its overlaps with two neighbouring particles increase. In addition, we study a more complex case by adding two more spheres added along the *y*-axis, as shown in Fig. 5b, in order to better resemble a typical confining situation. By studying these cases we can meticulously examine how deformation develops under different contact laws.

3.4.1 Test cases using hydrogel

The systems examined in the following contain $N = 3$ and $N = 5$ particles with radii $r = 1$ cm. The typical contact duration is $t_c = 2.87\left(\frac{(m_{ij})^2}{v_{max} r_{ij} (E^*)^2}\right)^{\frac{1}{5}}$ [48], with $m_{ij} = \frac{m_i m_j}{m_i + m_j}$ as the effective mass and v_{max} as the maximum relative velocity which leads to $t_c = 0.0018$s. Accordingly an integration time-step of $\Delta t = 0.00001$s ($t_c \gg \Delta t$, in order to allow for "safe" integration of the equations of motion) is chosen for simulations. Figure 6 shows the kinetic energy of systems

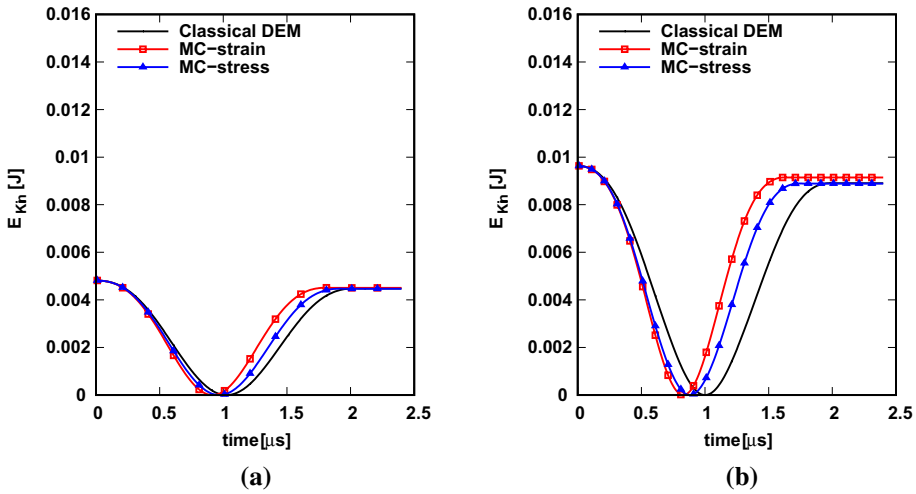

Fig. 6 Kinetic energy of test cases of **a** three and **b** five hydrogel spheres using different contact models as indicated in the inset

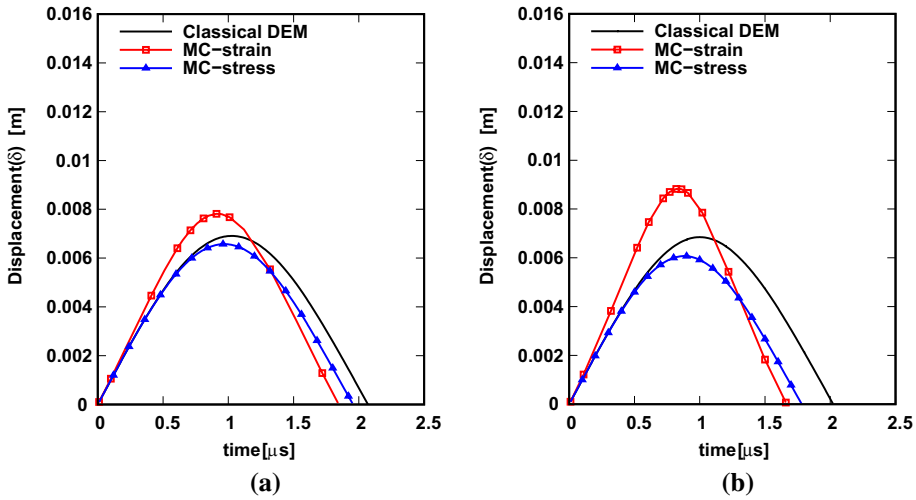

Fig. 7 Overlap of central particle for the test cases of **a** three and **b** five hydrogel spheres using different contact models as indicated in the inset

simulated by three and five hydrogel particles. Overlap of the central particle in case of three and five particles simulation are given in Fig. 7.

Looking at Fig. 6, we can see a faster reduction of the energy with the multi-contact implementations followed by an increase in the energy after the maximum indentation is reached (zero velocity). The shift of energy is related to the fact that the multi-contact models reach the maximum overlap earlier than the conventional model. The total forces acting on a single particle are gradually higher using multi-contact models.

It is clear that for higher total forces ($\Delta t, m$ = constant) we have lower magnitudes of the velocity and as a consequence less change in a particle's position. We can say that for multi-contact models, we have lower velocities when particles are compressed due to higher resistance and higher velocities at the decompression due to higher repulsive forces.

Overlap figures reveal that the contact collision is shorter while using multi-contact models since more resistance is applied against further compression. The maximum overlap of the MC-strain contact model is the highest in comparison to the two others due to the generation of new overlaps at each time step, i.e. in MC-strain model a "correction" term of the overlap is added. Contradictorily, the MC-stress model resists against compression (and decompression) which leads to a lower value of maximum overlap in comparison to other cases.

3.4.2 Test cases using rubber

In addition to hydrogel tests, we examine the three and five particles tests using a harder material (rubber) to confirm that the earlier observations remain independent of the particles properties. The contact duration of $t_c = 0.0025$s and an integration time-step of $\delta t = 0.00002$s are considered in simulations using rubber particles. Likewise the hydrogel tests, we can see that the kinetic energy plots show the same trend with stronger dissipation of energy while multi-contact

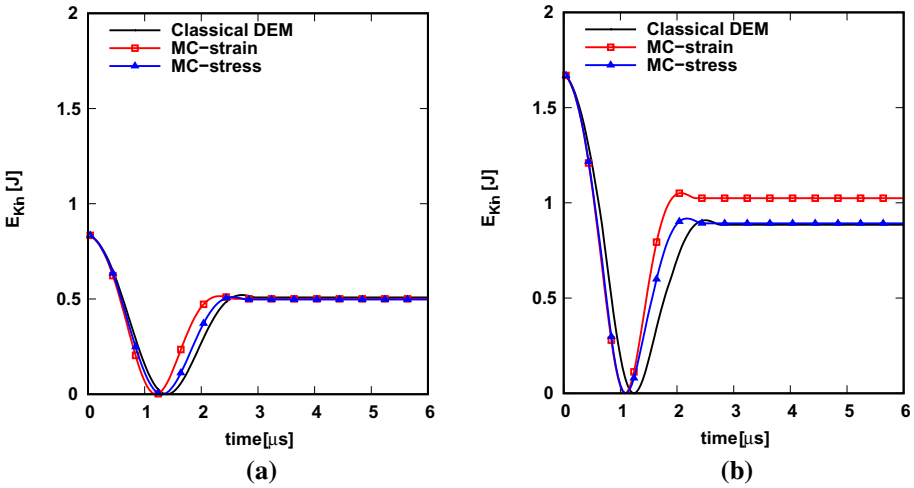

Fig. 8 Kinetic energy of test cases of **a** three and **b** five rubber spheres using different contact models as indicated in the inset

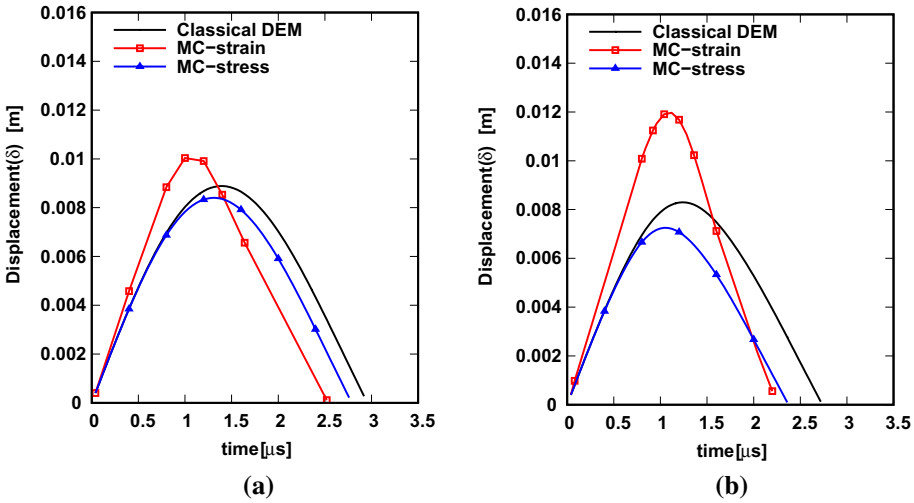

Fig. 9 Overlap of central particle for the test cases of **a** three and **b** five rubber spheres using different contact models as indicated in the inset

models are used (Fig. 8). Interestingly when our system gets more confined the reduction of the kinetic energy is the same for both multi-contact models (Fig. 8b) and the increase of the kinetic energy is higher due to the higher repulsive forces acting on a particle by applying MC-strain model. As it is observed in Fig. 9, the maximum overlap at the peak is reached by the MC-strain model, and the minimum is given by the MC-stress. It is not surprising since the basis of MC-strain is on adding new overlaps, and MC-stress is on correcting the force by adding new forces, i.e. stiffening of particles.

The results of test cases using hydrogel and rubber properties evidently show that the performance of multi-contact models is strongly dependent upon the confinement level of a system. However, it is hard to say which model shows a more robust agreement without comparing them to experimental data. Therefore, in the next sections we will compare different models for real tests of uniaxial compression.

3.4.3 Comparison with analytical formulation

The case of particles on a square regular lattice can be solved analytically [31]. Here, we solve our 5-particle test case analytically to compare with outputs of the proposed model.

Assume a constant isotropic strain ε_v that brings the particles from just touching to average overlap $\delta_4 = \varepsilon_v d$, where d is their typical diameter.

In this case, every particle will experience a pressure, $P_4 = (4/V)f(\delta_4)d = (4dk_H/V)\delta_4^{3/2}$, where $k_H = f_H/\delta^{3/2}$. The resulting corrected force is then:

$$f = f_H + (\beta\nu A_{ij})P_4 = k_H\delta_4^{3/2}[1 + 4d\beta\nu A_{ij}/V] \tag{11}$$

with $A_{ij} = \pi r_{ij}\delta_4$

The test case of 5-particle is compressed under constant engineering strain from an initial bounding box [− 0.03, 0.03; − 0.03, 0.03; − 0.01, 0.01;] to a final bounding box

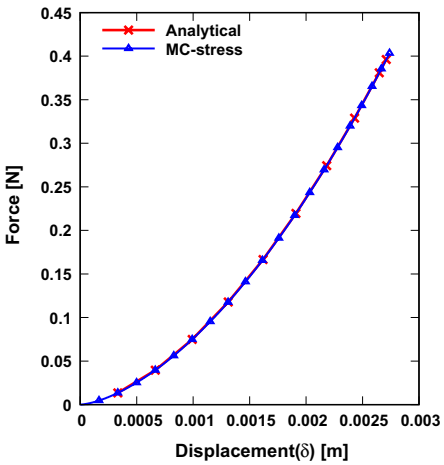

Fig. 10 Analytical solution of the MC-stress contact model

$[-0.025, 0.025; -0.025, 0.025; -0.01, 0.01]$. Knowing the strain field and using aforementioned relation between contact area and volumetric strain, one can obtain an analytical solution of this test case. Figure 10 shows the comparison between MC-stress and analytical solution. It is clear that DEM data using the MC-stress model follows the expected behavior of analytical solution, which validates not only the implementation of the model but also the accuracy of the model.

4 Uniaxial confined compression

After the validation of the new approach in the previous section, here, we simulate a more complex system which contains many particles and applying different contact models. The objective of this section is to encounter how our model is performing in comparison to existing models (classical DEM and MC-strain) and available experimental data given in Ref. [23]. The system considered here is a rectangular box, with dimension of $0.165 \times 0.165 \times 0.167$ m^3 along $x - y - z$ directions in which 514 polydisperse balls with a mean diameter of 2.1 cm were placed. The sample was first compressed uniaxially along the z-direction to a maximum target strain; after that it was decompressed.

4.1 Compression using hydrogel balls

We first consider hydrogel properties (given in Table 1) as the material characteristic of balls in the simulation. Results are compared with the existing experimental data. Figure 11 shows the results obtained from the compression/decompression simulation of the box filled with hydrogel spheres. It is not surprising to see the classical DEM fails in representing the experimental data, especially in case of hydrogel particles since it can not treat soft materials. The MC-stress model with a prefactor of $\beta = 1$ offers a fair performance, but not as good as the MC-strain model with a prefactor of $\gamma = 1$. Yet, we are far from describing the experimental data with these parameters presented in Fig. 11. To obtain a better agreement between simulation and experiment, one can tune the prefactors, γ and β, in both models. Calibration of these parameters were explained earlier in Sect. 3.3. The fitting parameters (γ and β) depend on material properties, especially on material stiffness. The calibration is ideally universal and should be done once for a given material and then be used for other tests without re-calibration. We show this below in Sect. 4.1.1, where another set of simulation is considered using the calibrated parameters.

A very good agreement between experimental and simulation data is obtained for MC-stress model by choosing $\beta = 1.65$ and shown in Fig. 11b. Although, setting $\gamma = 1.12$ which is the best fitting parameter for the case of MC-strain

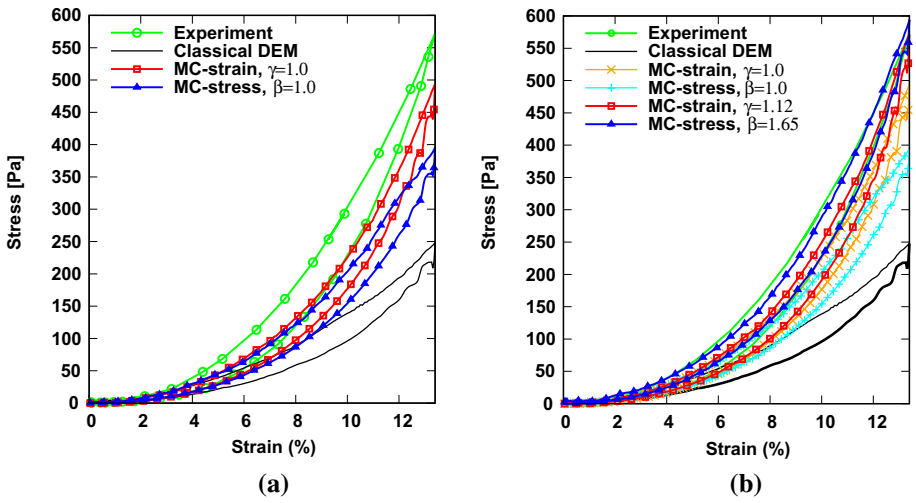

Fig. 11 Stress–strain response during compression-decompression of 514 hydrogel spheres with prefactors of **a** $\beta, \gamma = 1$, and **b** $\beta = 1.65, \gamma = 1.12$

model, as suggested by Ref. [49], shows a reasonable agreement but the representation is not good enough.

Furthermore, all contact forces between particles were visualized to establish the network of force chains and show the differences between examined models in micromechanical level. Figures 12 and 13 show the contact forces between particles, for the initial configuration and for the maximum engineering strain at 13.4%. Each contact force is drawn as

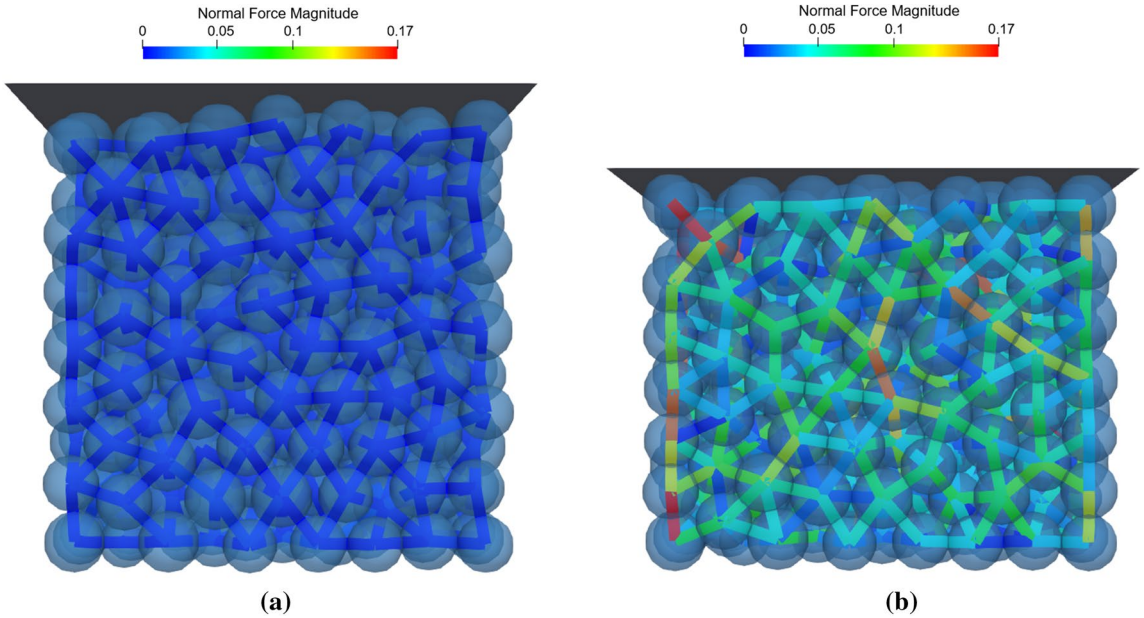

Fig. 12 (Color online) Contact forces between particles of the particle assembly. The color of the force represents the magnitude of normal force, with light (red online) corresponding to large forces down to blue (blue online) representing zero forces. Network of force chains **a** initial configuration, **b** normal contact forces computed at the maximum engineering strain with classical hertz contact model

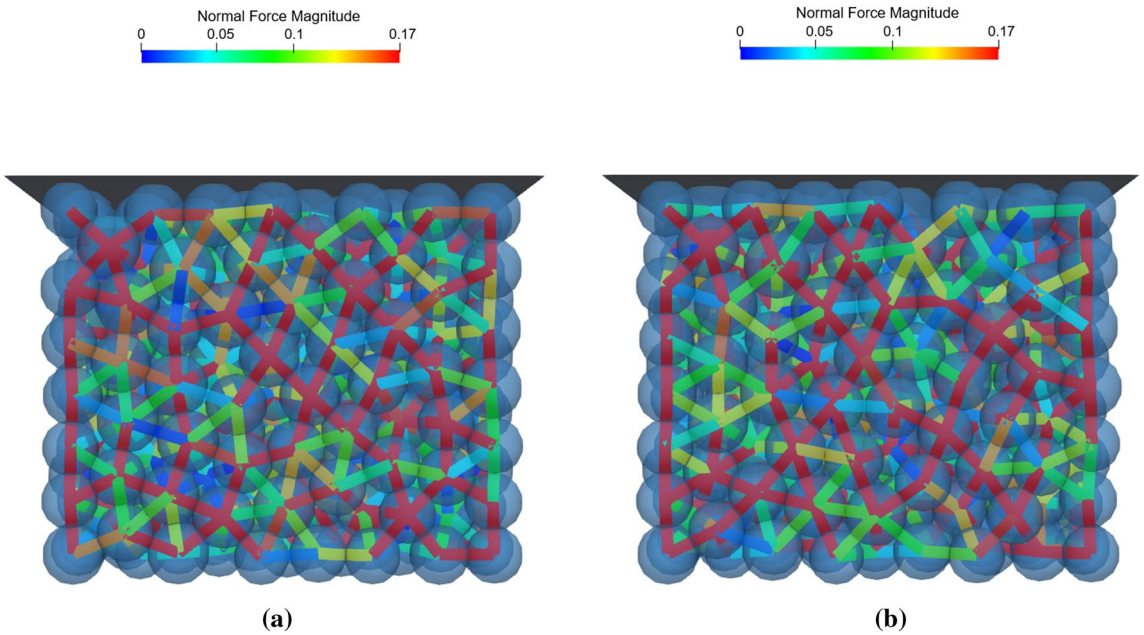

Fig. 13 (Color online) Contact forces between particles of the particle assembly. The color of the force represents the magnitude of normal force, with light (red online) corresponding to large forces down to blue (blue online) representing zero forces. Network of force chains for normal contact forces computed at the maximum engineering strain with **a** MC-strain contact model with $\gamma = 1.12$, **b** MC-stress contact model with $\beta = 1.65$

a line, with the color of the line representing the magnitude of the normal force. The difference between force networks achieved by the classical and multi-contact implementations is clear, with higher normal forces for the multi-contact implementations. Distributions of normal contact forces are also different between the two multi-contact models.

4.1.1 Compression using a different case of hydrogel spheres

For the calibrated parameters $\gamma = 1.12$ and $\beta = 1.65$ obtained from the case of 514 hydrogel spheres the objective of this section is to show how the multi-contact models are performing for a different case.

The system considered here is a rectangular box, with dimension of $0.165 \times 0.165 \times 0.147$ m^3 along $x - y - z$ directions in which 1573 hydrogel balls with a mean diameter of 1.6 cm and 348 hydrogel balls with a mean diameter of 2.1 cm were placed. The sample was compressed uniaxially along the z-direction to a maximum target strain of 10.2%. The simulation results are compared in Fig. 14 with experimental data reported in Ref. [50]. As expected the classical DEM is failing to reproduce the experimental data. However, a good agreement between experimental and simulation data is obtained for MC-stress model with $\beta = 1.65$; also, the MC-strain model with $\gamma = 1.12$ shows a reasonable agreement. This can reveal that MC-stress and MC-strain models can predict material behavior under similar but different conditions after a calibration step is conducted.

4.2 Compression using rubber spheres

In addition to the hydrogel simulations, we perform a numerical study employing rubber particles in order to see the performance of the multi-contact models in case of harder material which brings a higher level of confinement. Simulation setup is identical to the previous test (Sect. 4.1) with an only difference in the maximum strain level, up to 28%. The force displacement plot for a box filled with rubber particles is shown in Fig. 15. As expected, the MC-stress provides a higher maximum force with respect to the MC-strain and typical DEM.

4.3 Compression using glass beads

The system considered here is a cylinder, with a diameter of 12 mm and a height of 10.5 mm, in where 17 glass beads with a mean diameter of 3.9 mm (min: 3.8 mm, max: 4.0 mm) were located. Glass properties applied for the simulations are shown in Table 1. The objective of this case is to show how multi-contact models are performing while compressing stiff materials under high stresses and compare the results with our generated experimental data. It is worth mentioning that, since glass beads are brittle, the elastic part is the only focus here.

Figure 16 shows the results obtained from experimental and simulated compression of a cylinder filled with glass beads. Interestingly, we can see that the classical DEM is failing to resemble experimental data even for really small deformation (maximum strain 2.6%). The MC-strain model with a prefactor of $\gamma = 4.5$ offers a very good performance. The MC-stress model with a prefactor of $\beta = 5.17$ offers a slightly better performance and is able to capture the nonlinearity at high compression. Compared with previous cases we can see that prefactors γ and β are being set in high values, that is explained by the fact that for MC-strain model the displacement field $\delta_{k\to c}$ is in inverse proportion with the material Young's modulus (Eq. 7), therefore a stiffer

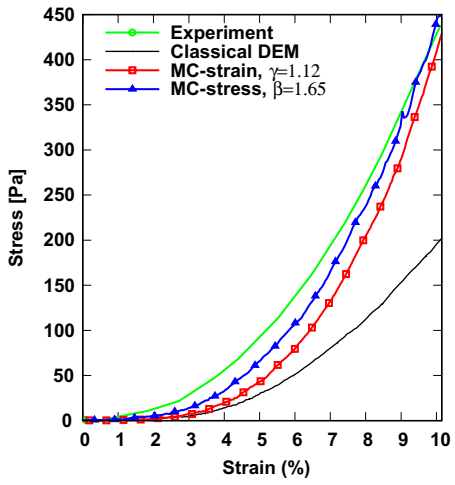

Fig. 14 Stress–strain response during compression of 1921 hydrogel spheres with prefactors of $\beta = 1.65$ and $\gamma = 1.12$

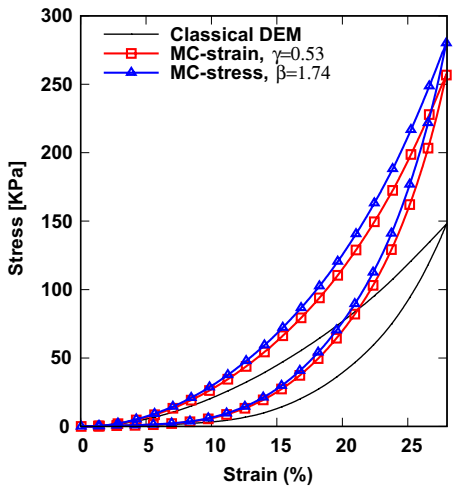

Fig. 15 Stress–strain response during compression of 514 rubber balls

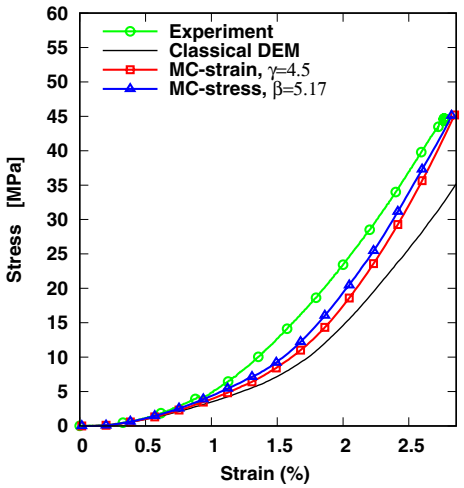

Fig. 16 Stress-strain response during compression of 17 glass beads until maximum strain 2.64%

Table 2 Computational time of uniaxial compression using different approaches

Model	T-hydrogel [s]	T-rubber [s]	T-glass [s]
Classical	38	84	22
MC-strain	668	1568	45
MC-stress	216	538	29

material will result in less forces than is required with prefactor $\gamma = 1$. As for the MC-stress model, and as we can see from Eq. 10, new forces are depending on the contact area between interacting particles, hence a stiffer material will result in less contact area. To compensate this the prefactor β should be set in a high value to capture the high forces of the examined case.

4.4 Computational cost performance of multi-contact models

Lastly, one of the advantage of the proposed multi-contact model (MC-stress) with respect to MC-strain is its computational time which is faster than MC-strain. For this reason, we address the computational time obtained during the uniaxial compression using different approaches in Table 2. It is not surprising that the classical DEM is much faster than the other two multi-contact models due to its simplicity, i.e. considering only independent pair contacts during its simulations. The success comes into the comparison of MC-stress and MC-strain models where the presented approach is faster than the MC-strain model.

5 Conclusions and outlooks

In this research, we studied the importance of multi-contact models to describe the behavior of dense strongly compressed granular materials. At first, a brief introduction to classical DEM was given. After that, a multi-contact model (MC-strain), which is based on the strain field around a particle, was explained. As an alternative, we proposed a new approach to consider the effect of surrounding particles based on the stress tensor applied on a particle (MC-stress).

Incorporating the multi-contact correction in classical DEM significantly improves the results (stress–strain) of dense packings of hydrogel (soft material) and glass (stiff material) particles under uniaxial compression calibrated by the experimental data of compression/decompression and the behavior of a single compressed rubber sphere. Similar to the MC-strain model, with our new multi-contact approach we included a prefactor β which must be carefully calibrated depending on the type of the material.

The new multi-contact approach is able to provide a higher force at a given displacement than the classical DEM and MC-strain when prefactors β and γ are set accordingly. A feature that allows us to remove the limits of classical DEM and accurately capture the required deformation. This might be also employed in pharmaceutical industry to model the tableting processes, where reaching extreme confinement under large applied engineering strain via DEM is still a challenge. In addition, we showed the simplicity of the new multi-contact model, which makes the model easy to implement and faster in comparison to existing multi-contact models (like MC-strain).

Next, one should conduct different types of experiments using a variety of materials (from soft to stiff) in order to allow for a wider comparison between our proposed model and experimental data. One can think of investigating the dependence of the model parameters on shape and mechanical properties of particles such as the elasto-plastic behaviour at high stress levels. For calibration, it would be interesting to provide these parameters by detailed finite elements simulations, where the deformation of particles is fully resolved.

Appendix

Pseudo-code used in the LIGGGHTS-DEM platform to obtain the global force acting on a particle.

```
for i = 1 to Nparticles do
    for j = 1 to Nneighbours do
        ForcesLocal [i,j] = Forces(Overlap[i, j]);
        StressTrace [i]+ = Stress(ForcesLocal[i, j], BranchVector[i, j]);
        StressTrace [j]+ = Stress(ForcesLocal[i, j], BranchVector[i, j]);
    end
end

for i = 1 to Nparticles do
    for j = 1 to Nneighbours do
        PressureSum [i,j]← 1/6 (StressTrace[i] + StressTrace[j]);
        ForcesGlobal [i,j]← Forces(Overlap[i, j], PressureSum[i, j]);
    end
end
```

Acknowledgements The economic support of the European Community under the Marie Sklodowska-Curie Initial Training Network FP7 (ITN607453) TMAPPP is gratefully acknowledged. We would like to thank the collaboration with Vanessa Magnanimo and A.H. Lasschuit. At the same time, the authors would also like to thank Benedikt Finke, Ramon Cabiscol, Dimitri Ivanov, Marcel Schrader, Christoph Thon and Clara Sangrós for their valuable input regarding the implementation of the code.

Compliance with ethical standards

Conflict of interest The authors that they do not have any conflicts of interest to declare.

References

1. Combe, G., Roux, J.N.: Good practice for sample preparation–construction of granular packings. ALERT Doctoral School 2017 Discrete Element Modeling, p. 99 (2017)
2. Luding, S.: Granular matter: so much for the jamming point. Nat. Phys. **12**(6), 531 (2016)
3. Cundall, P.A., Strack, O.D.L.: A discrete numerical model for granular assemblies. Geotechnique **29**(1), 47–65 (1979)
4. Martin, C.L., Bouvard, D., Shima, S.: Study of particle rearrangement during powder compaction by the discrete element method. J. Mech. Phys. Solids **51**(4), 667–693 (2003)
5. Senapati, R., Zhang, J.: Identifying fracture origin in ceramics by combination of nondestructive testing and discrete element analysis. In: AIP Conference Proceedings, vol. 1211. AIP, pp. 1445–1451 (2010)
6. Cleary, P.W., Sawley, M.L.: Dem modelling of industrial granular flows: 3d case studies and the effect of particle shape on hopper discharge. Appl. Math. Model. **26**(2), 89–111 (2002)
7. Cabiscol, R., Finke, J.H., Kwade, A.: Calibration and interpretation of DEM parameters for simulations of cylindrical tablets with multi-sphere approach. Powder Technol. **327**, 232–245 (2018)
8. Raji, A.O., Favier, J.F.: Model for the deformation in agricultural and food particulate materials under bulk compressive loading using discrete element method. I: theory, model development and validation. J. Food Eng. **64**(3), 359–371 (2004)
9. Luding, S.: Introduction to discrete element methods. basics of contact force models and how to perform the micro–macro transition to continuum theory. Eur. J. Environ. Civ. Eng. **12**(7–8), 785–826 (2008)
10. Harthong, B., Jérier, J.F., Dorémus, P., Imbault, D., Donzé, F.V.: Modeling of high-density compaction of granular materials by the discrete element method. Int. J. Solids Struct. **46**(18), 3357–3364 (2009)
11. Persson, A.S., Frenning, G.: An experimental evaluation of the accuracy to simulate granule bed compression using the discrete element method. Powder Technol. **219**, 249–256 (2012)
12. Gethin, D.T., Lewis, R.W., Ransing, R.S.: A discrete deformable element approach for the compaction of powder systems. Modell. Simul. Mater. Sci. Eng. **11**(1), 101 (2002)
13. Procopio, A.T., Zavaliangos, A.: Simulation of multi-axial compaction of granular media from loose to high relative densities. J. Mech. Phys. Solids **53**(7), 1523–1551 (2005)
14. Frenning, G.: An efficient finite/discrete element procedure for simulating compression of 3d particle assemblies. Comput. Methods Appl. Mech. Eng. **197**(49–50), 4266–4272 (2008)
15. Stransky, J.: Mesoscale Discrete Element Model for Concrete and Its Combination with FEM. PhD thesis, Czech Technical University in Prague (2018)
16. Nezamabadi, S., Radjai, F., Averseng, J., Delenne, J.Y.: Modeling soft granular media. In: Modeling Granular Media Across Scales-MGMAS2014 (2014)
17. Vu, T.L., Nezamabadi, S., Barés, J., Mora, S.: Analysis of dense packing of highly deformed grains. In: EPJ Web of Conferences, vol. 140. EDP Sciences, p. 15031 (2017)
18. Mora, S., Vu, T.L., Barés, J., Nezamabadi, S.: Highly deformed grain: from the hertz contact limitation to a new strain field description in 2d. In: EPJ Web of Conferences, vol. 140. EDP Sciences, p. 05011 (2017)
19. Iaconeta, I., Larese, A., Rossi, R., Oñate, E.: An implicit material point method applied to granular flows. Procedia Eng. **175**, 226–232 (2017)
20. Dosta, M., Costa, C., Al-Qureshi, H.: Numerical investigation of compaction of deformable particles with bonded-particle model.

In: EPJ Web of Conferences, vol. 140. EDP Sciences, p. 15021 (2017)
21. Haustein, M., Gladkyy, A., Schwarze, R.: Discrete element modeling of deformable particles in yade. SoftwareX **6**, 118–123 (2017)
22. Rojek, J., Zubelewicz, A., Madan, N., Nosewicz, S.: The discrete element method with deformable particles. Int. J. Numer. Methods Eng. **114**(8), 828–860 (2018)
23. Brodu, N., Dijksman, J.A., Behringer, R.P.: Multiple-contact discrete-element model for simulating dense granular media. Phys. Rev. E Stat. Nonlinear Soft Matter Phys. **91**(3), 1–6 (2015)
24. Gonzalez, M., Cuitiño, A.M.: A nonlocal contact formulation for confined granular systems. J. Mech. Phys. Solids **60**(2), 333–350 (2011)
25. Frenning, G.: Towards a mechanistic model for the interaction between plastically deforming particles under confined conditions: a numerical and analytical analysis. Mater. Lett. **92**, 365–368 (2013)
26. Celigueta, M.A., Latorre, S., Arrufat, F., Oñate, E.: Accurate modelling of the elastic behavior of a continuum with the discrete element method. Comput. Mech. **60**(6), 997–1010 (2017)
27. Karanjgaokar, N.: Evaluation of energy contributions using interparticle forces in granular materials under impact loading. Granul. Matter **19**(2), 36 (2017)
28. Johnson, K.L.: Contact Mechanics. Cambridge University Press, Cambridge (1987)
29. Thornton, C., Cummins, S.J., Cleary, P.W.: An investigation of the comparative behaviour of alternative contact force models during elastic collisions. Powder Technol. **210**(3), 189–197 (2011)
30. Taghizadeh, K., Luding, S., Magnanimo, V.: Dem applied to soil mechanics. In: ALERT Doctoral School 2017 Discrete Element Modeling, p. 129 (2017)
31. Luding, S.: Collisions & contacts between two particles. In: Physics of Dry Granular Media. Springer, pp. 285–304 (1998)
32. Li, Y., Xu, Y., Thornton, C.: A comparison of discrete element simulations and experiments for sandpiles composed of spherical particles. Powder Technol. **160**(3), 219–228 (2005)
33. Kruggel-Emden, H., Wirtz, S., Scherer, V.: A study on tangential force laws applicable to the discrete element method (DEM) for materials with viscoelastic or plastic behavior. Chem. Eng. Sci. **63**(6), 1523–1541 (2008)
34. Alenzi, A., Marinack, M., Higgs, C.F., McCarthy, J.J.: DEM validation using an annular shear cell. Powder Technol. **248**, 131–142 (2013)
35. Mindlin, R.D.: Elastic spheres in contact under varying oblique forces. J. Appl. Mech. **20**, 327–344 (1953)
36. Tsuji, Y., Tanaka, T., Ishida, T.: Lagrangian numerical simulation of plug flow of cohesionless particles in a horizontal pipe. Powder Technol. **71**(3), 239–250 (1992)
37. Di Renzo, A., Di Maio, F.P.: An improved integral non-linear model for the contact of particles in distinct element simulations. Chem. Eng. Sci. **60**(5), 1303–1312 (2005)
38. Thornton, C., Cummins, S.J., Cleary, P.W.: An investigation of the comparative behaviour of alternative contact force models during inelastic collisions. Powder Technol. **233**, 30–46 (2013)
39. Shäfer, J., Dippel, S., Wolf, D.E.: Force schemes in simulations of granular materials. J. Phys. I **6**(1), 5–20 (1996)
40. Silbert, L.E., Ertaş, D., Grest, G.S., Halsey, T.C., Levine, D.: Geometry of frictionless and frictional sphere packings. Phys. Rev. E **65**(3), 031304 (2002)
41. Greaves, G.N., Greer, A.L., Lakes, R.S., Rouxel, T.: Poisson's ratio and modern materials. Nat. Mater. **10**(11), 823–837 (2011)
42. Zhang, J., Behringer, R.P., Goldhirsch, I.: Coarse-graining of a physical granular system. Prog. Theor. Phys. Suppl. **184**, 16–30 (2010)
43. Labra, C., Ooi, J.Y., Sun, J.: Spatial and temporal coarse-graining for DEM analysis. In: AIP Conference Proceedings, vol. 1542. AIP, pp. 1258–1261 (2013)
44. Kloss, C., Goniva, C., Hager, A., Amberger, S., Pirker, S.: Models, algorithms and validation for opensource DEM and CFD–DEM. Prog. Comput. Fluid Dyn. Int. J. **12**(2–3), 140–152 (2012)
45. Plimpton, S.: Fast parallel algorithms for short-range molecular dynamics. J. Comput. Phys. **117**(1), 1–19 (1995)
46. Tatara, Y.: Extensive theory of force-approach relations of elastic spheres in compression and in impact. J. Eng. Mater. Technol. **111**(2), 163–168 (1989)
47. Brodu, N., Dijksman, J.A., Behringer, R.P.: Spanning the scales of granular materials through microscopic force imaging. Nat. Commun. **6**, 6361 (2015)
48. He, A., Wettlaufer, J.S.: Hertz beyond belief. Soft Matter **10**(13), 2264–2269 (2014)
49. Kloss, C.: Source code for MC-DEM simulations and simulation setup for hydrogel multicontact example. https://github.com/CFDEMproject/LIGGGHTS-PUBLIC (2017). Accessed Jan 17, 2017
50. Barés, J., Brodu, N., Zheng, H., Dijksman, J.A.: Transparent experiments: releasing data from mechanical tests on three dimensional hydrogel sphere packings. Granul. Matter **22**(1), 21 (2020)